Applied Catalysis B: Environmental 152–153 (2014) 233–240

Contents lists available at ScienceDirect

Applied Catalysis B: Environmental

journal homepage: www.elsevier.com/locate/apcatb

Visible light photocatalysis of fullerol-complexed TiO_2 enhanced by Nb doping

Jonghun Lim[a], Damián Monllor-Satoca[a], Jum Suk Jang[a], Seockheon Lee[b], Wonyong Choi[a,*]

[a] School of Environmental Science and Engineering, Pohang University of Science and Technology (POSTECH), Pohang 790-784, Republic of Korea
[b] Center for Water Resources Cycle Research, Korea Institute of Science and Technology, Seoul 136-791, Republic of Korea

ARTICLE INFO

Article history:
Received 1 December 2013
Received in revised form 9 January 2014
Accepted 13 January 2014
Available online 22 January 2014

Keywords:
Visible light photocatalyst
Titanium dioxide
Surface-complex charge-transfer
Impurity doping
Degradation of water pollutants

ABSTRACT

Visible light photocatalysis by TiO_2 nanoparticles modified with both fullerol complexation and Nb-doping (fullerol/Nb–TiO_2) demonstrated an enhanced performance. Nb-doped TiO_2 (Nb-TiO_2) was firstly prepared by a conventional sol–gel method, and subsequently fullerol was adsorbed on the surface of Nb–TiO_2. The physicochemical and optical properties of as-prepared fullerol/Nb-TiO_2 were analyzed by various spectroscopic methods (TEM, EELS, XPS, and DRS). The adsorption of fullerol on Nb–TiO_2 surface increased the visible light absorption through a surface-complex charge-transfer (SCCT) mechanism. Nb-doping enhanced the charge transport and induced the Ti cation vacancies that retarded the recombination of photo-generated charge pairs by trapping the electrons injected from the HOMO level of fullerol. Due to the advantage of simultaneous modification of fullerol and Nb-doping, the visible light photoactivity of fullerol/Nb–TiO_2 was more enhanced than either Nb–TiO_2 or fullerol/TiO_2. The photocatalytic activities of fullerol/Nb–TiO_2 for the reduction of chromate (Cr^{VI}), the oxidation of iodide, and the degradation of 4-chlorophenol were all higher than bare TiO_2 and singly modified TiO_2 (*i.e.*, Nb–TiO_2 and fullerol/TiO_2) under visible light ($\lambda > 420$ nm). A similar result was also confirmed for their photoelectrochemical behavior: the electrode made of fullerol/Nb–TiO_2 exhibited an enhanced photocurrent under visible light. On the other hand, the decay of open-circuit potential of the fullerol/Nb–TiO_2 electrode after turning off the visible light was markedly slower than either that of Nb–TiO_2 or fullerol/TiO_2, which implies the retarded recombination of photo-generated charge pairs on fullerol/Nb–TiO_2. In addition, the electrochemical impedance spectroscopic (EIS) data supported that the charge transfer resistance is lower with the fullerol/Nb–TiO_2 than either Nb–TiO_2 or fullerol/TiO_2. This specific combination of the bulk (Nb-doping) and surface (fullerol complexation) modifications of titanium dioxide might be extended to other cases of bulk + surface combined modifications.

1. Introduction

Titanium dioxide (TiO_2) is a well-known wide bandgap photocatalyst that has been extensively studied for solar energy conversion (fuels, solar cells) [1,2] and a great variety of photocatalytic processes [3,4]. However, its photoactivity is mostly limited to the UV region because of its wide bandgap (3.0–3.2 eV). For many years, researchers have tried to expand its activity to the visible light region, as visible light accounts for 45% of incident solar energy. Various strategies have been attempted to induce visible light absorption [5–13]. One of the most popular methods is to modify the TiO_2 surface by attaching visible light-absorbing adsorbates (*e.g.*, dyes, surface complexes). In the case of dye sensitization, the photo-generated electrons are transferred from the excited dye LUMO (lowest unoccupied molecular orbital) level to the semiconductor (normally, conduction band states). On the other hand, the sensitization by surface complexes proceeds through a charge transfer (CT) mechanism between the surface adsorbate and semiconductor, in which the electron is photoexcited directly from the adsorbate ground-state (HOMO: highest occupied molecular orbital) to the semiconductor conduction band (CB). Such CT-complex formation on TiO_2 has been previously reported with catechol [14], fullerol ($C_{60}(OH)_x$) [15], 2,4-diisocyanate (TDI) [16], EDTA [17], metal cyanide [18], phenolic resin [19], to name a few examples. The visible light activation of wide bandgap semiconductors by the surface complex CT mechanism has been recently reviewed [20]. Although the mechanism of photoinduced electron transfer is different between the CT-surface complex (HOMO to TiO_2 CB) and dye sensitization (LUMO to TiO_2 CB), there are some similarities. For example, the CT-complex and dye should have the proper anchoring groups such as hydroxyl or carboxyl groups so that the chemical binding between the adsorbate

* Corresponding author. Tel.: +82 54 279 2283; fax: +82 54 279 8299.
E-mail address: wchoi@postech.edu (W. Choi).

0926-3373/$ – see front matter © 2014 Elsevier B.V. All rights reserved.
http://dx.doi.org/10.1016/j.apcatb.2014.01.026

molecule and the semiconductor surface is strong enough to induce the electronic coupling between the adsorbate orbital and the semiconductor CB states [21]. However, because of this strong electronic coupling, both CT-complexation and dye sensitization on TiO_2 suffer from the fast recombination between the injected electron and the oxidized adsorbate, which limits the overall photocatalytic activity [22].

The electrons injected into CB should be rapidly transported to reactive surface sites and the electron transport in metal oxide can be enhanced by doping foreign elements in the lattice of base materials. In this respect, Zn-, Al- and Nb-doped TiO_2 have been studied as base electrodes for dye-sensitized solar cells (DSSC) [23–25] and photocatalysts [26]. In particular, Nb doping in TiO_2 increases the electron concentration, conductivity and transport efficiency with enhancing the photocurrent because the additional electron is introduced through a charge compensation mechanism upon the ionic substitution of Nb^{5+} in a Ti^{4+} position (with reducing some Ti^{4+} to Ti^{3+}) [27,28]. Alternatively, the charge compensation can be achieved by creating Ti^{4+} vacancies in the lattice, which may serve as electron traps [25,29]. Furthermore, it has been proposed that the driving force for charge injection from the excited dye to Nb-TiO_2 in DSSC is enhanced and the recombination between the injected electron and the oxidized dye radical is retarded by a positive shift of flat band potential (V_{fb}), which is induced by Nb doping [25,29,30].

This study aimed to apply the Nb-doping effect to the CT-sensitization of TiO_2 under visible light. As a model system of CT-sensitization, fullerol ($C_{60}(OH)_x$) complexed on Nb–TiO_2 surface was selected. The CT-sensitization mechanism of fullerol/TiO_2 and its photocatalytic and photoelectrochemical (PEC) properties were previously investigated [15]. The activity of fullerol/Nb–TiO_2 sample was evaluated under ambient condition for the photocatalytic conversion of various substrates as well as its PEC performance under visible light. Significant improvements in the photocatalytic and PEC activities of fullerol/Nb–TiO_2 were observed compared with either fullerol/TiO_2 or Nb–TiO_2. The fullerol sensitization through surface complexation and the Nb doping effect on the interfacial charge transfer and recombination are discussed in detail to understand the advantage of modification of the dual components (fullerol and Nb dopant) in the CT-type visible light photocatalysis.

2. Experimental

2.1. Chemicals and materials

The chemicals used in this study were titanium tetraisopropoxide (TTIP, $Ti(OCH(CH_3)_2)_4$, Aldrich), Fullerol (polyhydroxyfullerene, $C_{60}(OH)_x$, x = 10–15, MER corporation), ethanol (Aldrich), niobium chloride ($NbCl_5$, Aldrich) and nitric acid (HNO_3, Shinyo). 4-chlorophenol (4-CP, Sigma), $Na_2Cr_2O_7$ (Cr^{VI}, Aldrich) and KI (Aldrich) were used as chemical substrates for photocatalytic activity tests. All chemicals were used as received without further purification. Deionized water used for solution preparation was ultrapure (14 MΩ cm) and prepared by a Barnstead purification system.

2.2. Preparation of photocatalysts

Bare TiO_2 and Nb-TiO_2 were prepared by a sol–gel method. For bare TiO_2, 1.25 mL of TTIP was dissolved in 25 mL of ethanol. This aqueous solution was then added dropwise to 250 mL of distilled water and its pH was subsequently adjusted to 1.5 with nitric acid. The resulting sol was stirred for 24 h, evaporated at 50 °C using a rotary evaporator, dried at 70 °C, calcined at 400 °C (heating ramp, 1 °C/min) and kept at this temperature for 3 h. As for the preparation of Nb-TiO_2, niobium chloride ($NbCl_5$) at various concentrations was added to the solution of TTIP and ethanol and the same procedure described above was followed.

Fullerol was adsorbed on the surface of bare TiO_2 and Nb–TiO_2 by following a reported method [15]. In brief, the as-prepared catalyst powder (0.1 g) was dispersed in an aqueous fullerol solution (100 mL, 45 μM) and buffered at pH 3 with $HClO_4$. The solution was stirred for 3 h, and then the catalyst was collected by filtering. After drying in an open-air oven (80 °C), a brownish powder was obtained.

2.3. Characterization of photocatalysts

The crystalline phase identification of as-made bare-TiO_2 and Nb–TiO_2 was carried out by X-ray diffraction (XRD) using the Cu $K\alpha$ radiation (Mac Science Co. M18XHF). Diffuse reflectance UV/visible absorption spectra (DRS) of powder samples were recorded using a spectrophotometer (Shimadzu UV-2401PC) with an integrating sphere attachment and $BaSO_4$ was used as the reference. The electron energy loss spectroscopy (EELS) analysis was obtained using a JEM-2100F microscope with Cs-corrected line. The surface chemical composition was analyzed by X-ray photoelectron spectroscopy (XPS, Kratos, XSAM 800 pci) with using Mg $K\alpha$ as an excitation line (1253.6 eV). The binding energy calibration was performed using the impurity C 1s peak present in the prepared sample as the reference energy (284.6 eV).

2.4. Photocatalytic activity tests

The visible light photoactivities of the synthesized samples were tested using the photocatalytic oxidation of 4-chlorophenol (4-CP), and iodide and the photoreduction of hexavalent chromate (Cr^{VI}). The as-prepared samples were dispersed in distilled water (0.5 g/L). An aliquot of substrate stock solution was added to the suspension and then the initial pH of the suspension was adjusted to 3.0 with a standard solution of $HClO_4$. The solutions were equilibrated in the dark for 30 min prior to visible light irradiation. Photo-irradiation was performed using a 300-W Xe arc lamp (Oriel) as a light source. Light passed through a 10-cm IR water filter and a cut-off filter (λ > 420 nm for visible light irradiation), and then the filtered light was focused onto a 30 mL Pyrex reactor with a quartz window. Sample aliquots were intermittently withdrawn from the reactor every 30 min during visible light irradiation and filtered through a 0.45 μM PTFE syringe filter (Millipore) to remove the photocatalyst particles. Multiple photocatalytic activity measurements were carried out under the identical experimental conditions to confirm the reproducibility. When the photocatalytic oxidation of iodide to triiodide (I_3^-) was tested, the triiodide production was monitored by measuring the spectrophotometric absorbance at 352 nm (ε = 26,400 M^{-1} cm^{-1}). The degradation of 4-CP and the concurrent production of chloride were monitored using a high performance liquid chromatography (HPLC, Agilent 1100 series) and an ion chromatograph (IC, Dionex DX-120), respectively. The concentration of Cr^{VI} was analyzed using a colorimetric method with 1,5-diphenylcarbazide (DPC) reagent [31]. The color change was monitored at 540 nm (ε = 6,850 M^{-1} cm^{-1}) using a UV/Visible spectrophotometer (Agilent 8453).

2.5. Photoelectrochemical measurements

All PEC measurements were carried out using a standard three-electrode cell connected to a computer-controlled potentiostat (Gamry, Reference 600). The PEC cell consisted of a photoanode of fullerol/Nb-TiO_2, a Ag/AgCl (saturated KCl) reference electrode and a platinum wire (for Mott–Schottky plot and electrochemical

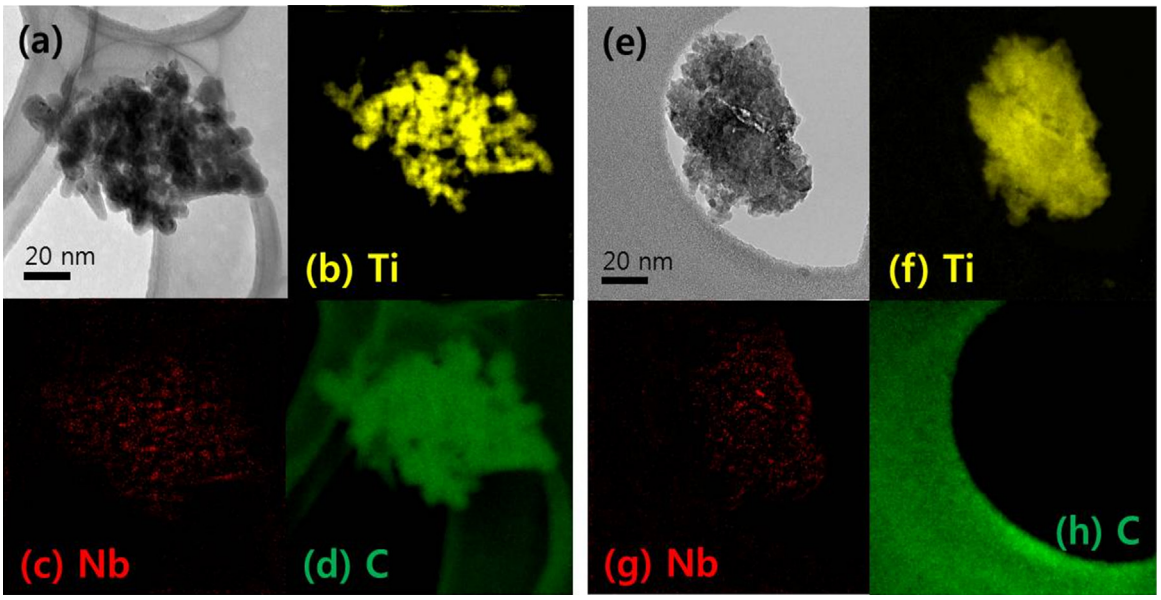

Fig. 1. (a) TEM image of fullerol/Nb–TiO_2 and EELS mapping of (b) Ti, (c) Nb, (d) C on fullerol/Nb–TiO_2, (e) TEM image of Nb–TiO_2 and EELS mapping of (f) Ti, (g) Nb, (h) C on Nb–TiO_2.

impedance spectra (EIS)) or graphite rod (for photocurrent and photovoltage measurement) as a counter electrode. The photoanode was fabricated using Carbowax as a binder. The as-prepared TiO_2 or Nb-TiO_2 was added to a mixture of poly(ethylene glycol) (PEG, Aldrich) and distilled water (50 wt%) and coated on an FTO plate using the doctor-blade method with tracks of two strips of Scotch tape. Then, the coated electrode was calcined at 450 °C for 1 h to burn out the organic binder and cooled down to room temperature. It was then immersed into the acidic solution of fullerol (45 μM) over 12 h to make the electrode of fullerol/TiO_2 and fullerol/Nb-TiO_2. The photoanode in the PEC cell was immersed in $NaClO_4$ solution (0.2 mM, Aldrich) and biased at +0.6 V (*vs.* Ag/AgCl) during photocurrent and 0 V (*vs.* Ag/AgCl) during EIS measurements. The solution was magnetically stirred during all PEC measurements. To confirm the positive shift of CB, flat band potentials (V_{fb}) measurements were carried out with using the Mott–Schottky plot. The experiment was performed in aqueous 0.1 M Na_2SO_4 solution in the dark. The potential was varied between 0 and −1 V (*vs.* Ag/AgCl) with an AC amplitude of 10 mV and frequencies in the 500–3000 Hz range.

3. Results and discussion

3.1. Characterization of photocatalysts

The crystallographic phase of the as-prepared samples was identified by powder XRD. All samples are in the anatase phase, indicating that the doping of Nb and the hybridization with fullerol did not induce any phase transition (see Fig. S1) The 0.5 at% Nb-doped sample was characterized and analyzed in most cases because this composition exhibited the highest photocatalytic activity among the doped samples with different niobium concentrations (*vide infra*). To confirm the existence of Ti, C and Nb within the samples, elemental EELS analysis was performed and shown in Fig. 1. The elemental mapping analysis clearly exhibits the difference between fullerol/Nb-TiO_2 (Fig. 1a–d) and Nb-TiO_2 (Fig. 1e–h). The uniform distribution of Ti, C and Nb was confirmed in fullerol/Nb-TiO_2 particles, whereas the Nb-TiO_2 image shows the absence of carbon. The presence of these elements could be further confirmed by XPS. As shown in Fig. 2a, there are three major peaks of C 1s which are centered at 284.5, 287.0 and 288.7 eV. Among them, the peak at 284.5 eV is observed in all samples and is ascribed to ambient organic impurities adsorbed on the surface of catalyst samples [32]. However, the intensities of the peaks at 287.0 and 288.7 eV corresponding to oxidized carbon species such as C(O)OH, C=O and C–O [33] evidently increased in the presence of fullerol adsorbed on the bare- and Nb–TiO_2. Fullerol molecules ($C_{60}(OH)_x$) have many hydroxyl groups through which CT-complexes can be formed on the titania surface (reaction (1)) [15].

$$C_{60}(OH)_x + \equiv Ti - OH \quad \rightarrow \quad \equiv Ti - O - C_{60}(OH)_{x-1} + H_2O \qquad (1)$$

Consequently, the surface complexation of fullerol on bare- and Nb–TiO_2 might influence the binding energy of O 1s. As shown in Fig. 2b, the binding energy profiles of O 1s peak in the absence and presence of fullerol are clearly different. When fullerol was adsorbed on bare- and Nb–TiO_2, the peak intensity at 531.3 eV (ascribed to Ti–OH) decreased while that at 533.5 eV (attributed to C–OH) increased. The reduced intensity of titanol O peak upon complexation with fullerol indicates the condensation reaction of the surface hydroxyl groups with fullerol (reaction (1)) [34]. The XPS spectra of Nb 3d (see Fig. 2c) in doped TiO_2 show the peak position at 207.8 eV, which corresponds to Nb^{5+} species (bulk Nb_2O_5) [35]. The above EELS and XPS analysis results confirm the surface complexation of fullerol on TiO_2 and the Nb doping in TiO_2.

Fig. 3 shows the diffuse reflectance UV/Visible spectra (DRS) of Nb-doped TiO_2 samples with (Fig. 3a) and without (Fig. 3b) the surface-complexed fullerol. When fullerol was adsorbed on the surface of Nb-TiO_2, the visible light absorption was markedly enhanced through a charge transfer mechanism [15], which involves a visible light-induced transition from HOMO of fullerol to TiO_2 CB. As Nb concentration increased, the absorption edge was slightly red-shifted (lower E_g) in both cases (with and without fullerol). The introduction of Nb^{5+} in TiO_2 lattice may induce the charge compensation upon the substitution of Ti^{4+} sites and create a donor level located closer to the conduction band [36]. As a result, the absorption edge might be slightly red-shifted. To understand the slightly reduced bandgap upon Nb doping, we analyzed the Mott–Schottky plot because the CB edge can be estimated from the flat-band potential (V_{fb}) (if we assume that the difference between V_{fb} and CB minimum is negligible for n-type semiconductors) [37,38].

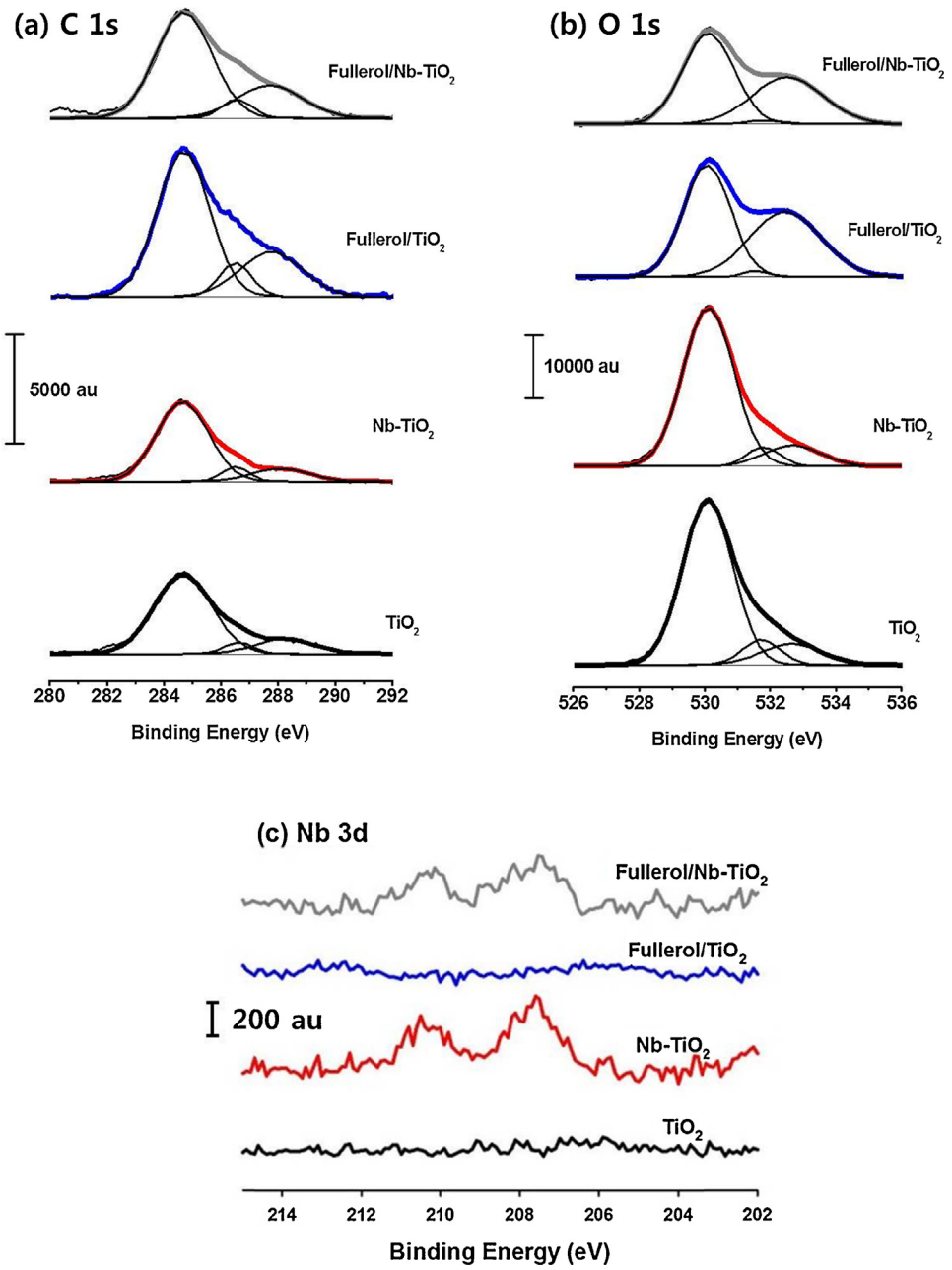

Fig. 2. XPS spectra of (a) C 1s, (b) O 1s and (c) Nb 3d signals in bare TiO_2, Nb–TiO_2, fullerol/TiO_2 and fullerol/Nb–TiO_2.

Fig. 4 shows that V_{fb} is positively shifted with increasing the Nb concentration. This implies that the bandgap of Nb-TiO_2 was reduced by the positive shift of CB edge, which is induced by the substitution of Ti^{4+} with Nb^{5+} [29,39]. However, the fullerol complexation on TiO_2 and Nb–TiO_2 did not affect the flat-band potential as shown in Fig. S2.

In addition to the "fullerol-to-CB CT" in the fullerol/TiO_2 system, alternative CT transition from fullerol HOMO to the Nb-induced defect levels might be also possible in the fullerol/Nb-TiO_2. The proposed CT transitions are schematically illustrated in Scheme 1. The presence of this CT effect (fullerol-to-defects; indicated as CT_2 in Scheme 1) can be supported by the absorption spectra of fullerol/Nb-TiO_2 (see Fig. 3b): the visible light absorption background in the range of 450–600 nm monotonously increases with increasing the Nb dopant concentration although Nb–TiO_2 alone cannot absorb in this region at all. The difference spectrum between the fullerol/TiO_2 and fullerol/Nb(5%)–TiO_2 (solid red line in Fig. 3c) and that between the undoped TiO_2 and Nb(5%)-TiO_2 (dashed black line in Fig. 3c) clearly show the synergic effect of Nb dopant on the fullerol-induced visible light absorption. Since the energy levels of the Nb-induced defects are located closely below the CB minimum, the CT_2 transition (fullerol-to-defect) requires slightly lower energy than the CT_1 transition (fullerol-to-CB). As a result, the absorption spectrum of the CT_2 transition is expected to be red-shifted from that of the CT_1 transition with elevating the visible light absorption background, which is actually observed in Fig. 3b.

3.2. Photocatalytic and photoelectrochemical properties of fullerol/Nb–TiO_2

In order to evaluate the photocatalytic activity of fullerol/Nb–TiO_2 under visible light, as-prepared samples were tested using chromate (Cr^{VI}), iodide (I^-) and 4-CP as test substrates in water. Prior to irradiation, all substrates were equilibrated for

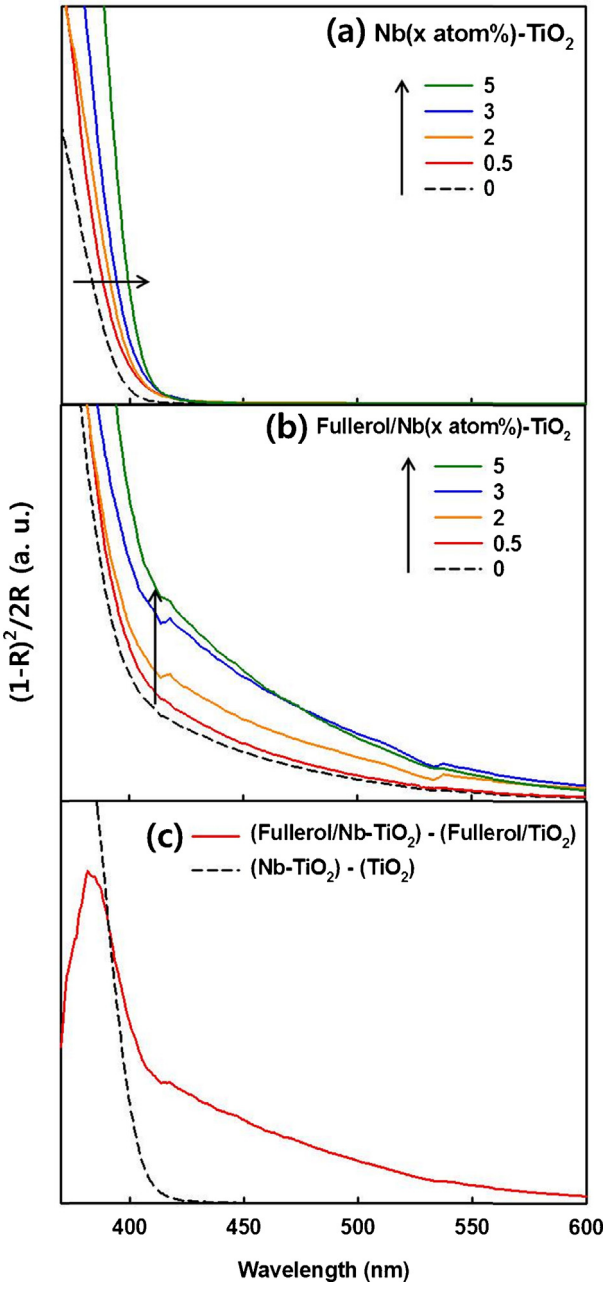

Fig. 3. Diffuse reflectance UV/visible spectra of (a) Nb(x at%)-TiO_2 and (b) fullerol/Nb(x at%)–TiO_2, (c) Difference spectra between fullerol/Nb(5%)–TiO_2 and fullerol/TiO_2 and that between Nb(5%)–TiO_2 and undoped TiO_2.

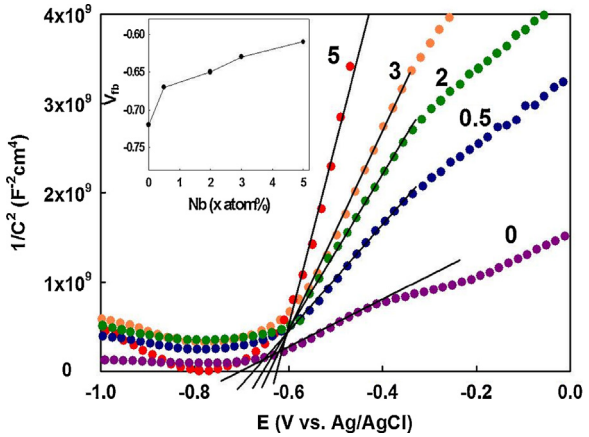

Fig. 4. Mott–Schottky plot of Nb(x at%)-TiO_2. Inset the flat band potentials (V_{fb}) of Nb-TiO_2 as a function of the Nb dopant concentration. The Mott–Shottky plot was measured in the dark with an aqueous electrolyte of 0.1 M Na_2SO_4.

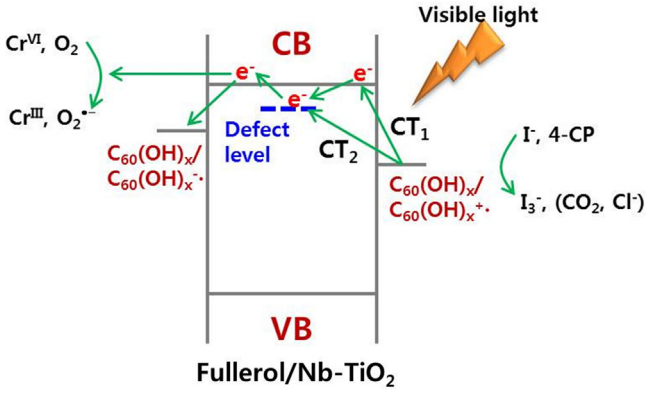

Scheme 1. Schematic illustration for the photocatalytic reduction (Cr^{VI}) and oxidation (I^-, 4-CP) reactions occurring on fullerol/Nb-TiO_2 through charge-transfer (CT) mechanism under visible light irradiation.

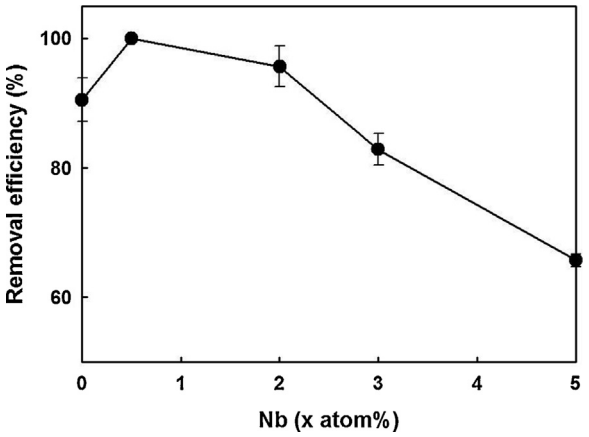

Fig. 5. Photocatalytic removal efficiency for the reduction of Cr^{VI} (hexavalent chromium) as a function of the Nb concentration in fullerol/Nb(x at%)–TiO_2 under visible light irradiation for 90 min. Experimental conditions: [catalyst] = 0.5 g/L, $[Cr^{VI}]_0$ = 200 μM, pH_i = 3.0, λ > 420 nm, air-equilibrated for 30 min prior to irradiation.

30 min to ensure the pre-adsorption on the catalyst surface. First, Nb–TiO_2 with various Nb levels was tested to find the optimum dopant concentration for the photocatalytic reduction of Cr^{VI} to Cr^{III} (Fig. 5). The TiO_2 sample doped with 0.5 at% Nb exhibited the highest photoactivity under visible light, which is consistent with the previous works [25,40]. Further increasing the concentration of Nb dopant above 2 at% decreased the activity to the level even lower than the undoped sample. Thus the dopant concentration was fixed at 0.5 at% for further activity tests.

Fig. 6 compares the time profiles of the photocatalytic conversion of Cr^{VI}, I^- and 4-CP in aqueous suspensions of bare TiO_2, Nb–TiO_2, fullerol/TiO_2 and fullerol/Nb–TiO_2. In all cases, fullerol/Nb–TiO_2 exhibited the higher activities than either Nb–TiO_2 or fullerol/TiO_2, which confirms that both photo-oxidative and photo-reductive conversions are enhanced by the simultaneous modification with Nb dopant and fullerol complexation. The photo-reduction of chromate by bare TiO_2 was insignificant because CB electrons cannot be generated under visible light. The photoactivity of Nb–TiO_2 was also low, which is ascribed to weak absorption of visible light (see Fig. 3a) but fullerol

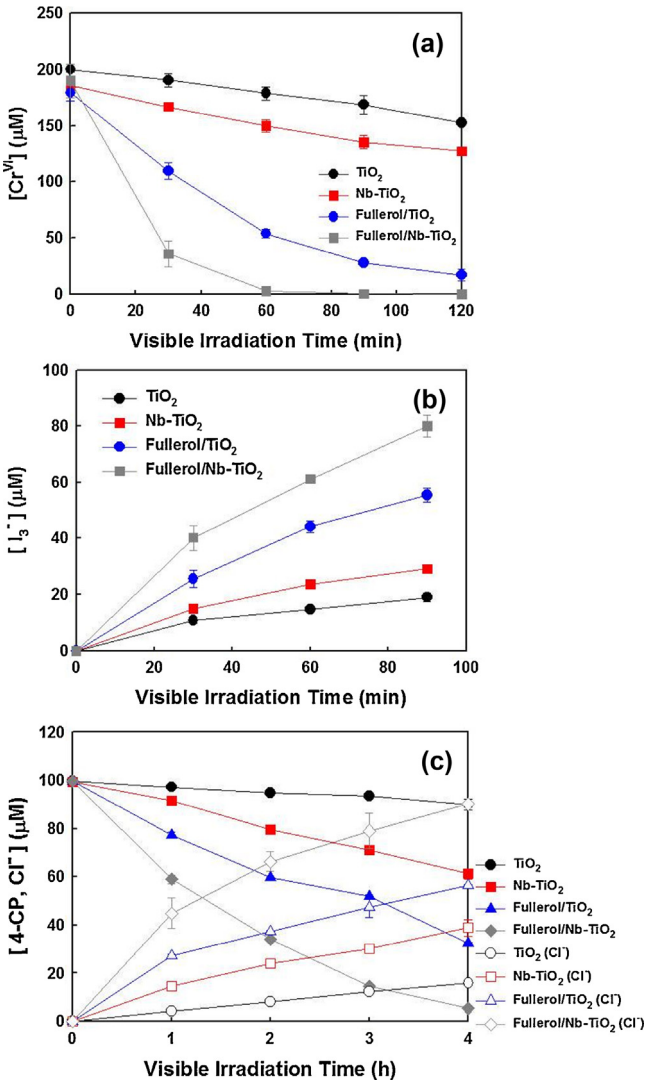

Fig. 6. Time profiles of photocatalytic (a) removal of Cr^{VI} through reduction, (b) production of triiodide from the oxidation of I^- and (c) degradation of 4-CP with the accompanying production of chloride in the illuminated catalyst slurries. The experimental conditions were [catalyst] = 0.5 g/L, $[Cr^{VI}]_0$ = 200 μM, $[I^-]_0$ = 10 mM, $[4\text{-CP}]_0$ = 100 μM, pH_i = 3.0, λ > 420 nm, air-equilibrated for 30 min prior to irradiation.

complexation markedly increased the visible light absorption of TiO_2 through the CT mechanism (reaction (2)), which subsequently leads to the reduction of chromate (reaction (3)).

$$\equiv Ti - O - C_{60}(OH)_{x-1} + h\nu \rightarrow \left[\equiv Ti - O - C_{60}(OH)_{x-1}\right]^{\bullet+} + e_{cb}^- \quad (2)$$

$$3e_{cb}^- + Cr^{VI} \rightarrow Cr^{III} \quad (3)$$

$$\left[\equiv Ti - O - C_{60}(OH)_{x-1}\right]^{\bullet+} + e_{cb}^- \rightarrow \equiv Ti - O - C_{60}(OH)_{x-1} \quad (4)$$

$$e_{cb}^- + \square_{Ti}(Ti\ \ vacancy) \rightarrow e_{tr}^- \quad (5)$$

$$\left[\equiv Ti - O - C_{60}(OH)_{x-1}\right]^{\bullet+} + e_{tr}^- \rightarrow \equiv Ti - O - C_{60}(OH)_{x-1}\ (slower\ than\ reaction\ (4)) \quad (6)$$

$$\left[\equiv Ti - O - C_{60}(OH)_{x-1}\right]^{\bullet+} + D(substrate) \rightarrow \equiv Ti - O - C_{60}(OH)_{x-1} + D^{\bullet+} \quad (7)$$

$$e_{cb}^- + O_2 \rightarrow O_2^{\bullet-} \quad (8)$$

$$e_{cb}^- + 2H^+ + O_2^{\bullet-} \rightarrow H_2O_2 \quad (9)$$

$$e_{cb}^- + H_2O_2 \rightarrow {}^{\bullet}OH + {}^-OH \quad (10)$$

As a result, the visible light photoactivity of fullerol/TiO_2 was higher than bare TiO_2 and Nb–TiO_2. The activity of fullerol/Nb–TiO_2 for Cr^{VI} reduction was further enhanced by Nb doping as compared to fullerol/TiO_2. Nb-doping in TiO_2 can increase the CB electron concentration and conductivity by inducing new donor levels [40]. On the other hand, it can also reduce the recombination of charge pairs (reaction (4)) by trapping electrons in the Ti cation vacancy level introduced near the CB (reactions (5) and (6)) [41]. As these effects of Nb-doping were applied to DSSC to increase the efficiency, they can be applied to the CT-type visible active photocatalysis as well. The excess electron generated by Nb-doping can accelerate the reduction of chromate by enhancing the electron transport. Therefore, fullerol/Nb–TiO_2 exhibited the highest photocatalytic activity for chromate reduction (Fig. 6a). However, the fact that increasing the Nb dopant above 2 at% has a significant negative effect on the visible light activity (see Fig. 5) implies that the excessive defect sites (induced by Nb dopants) should accelerate the recombination (reaction (4)). Increasing the concentration of Nb dopant above the optimal level should increase the concentration of both Ti vacancies (serving as electron trap sites) and CB electrons at the same time (*via* the different charge compensation mechanisms). Under such condition, the positive effects of Nb doping, which are the retardation of the recombination by electron trapping and the enhancement of electron conductivity, might be cancelled out. Therefore, it seems that both effects work together at the lower dopant concentration but counteract at the higher concentration.

The photocatalytic oxidation of iodide and 4-CP was also tested under visible light and similar results were obtained (Fig. 6b and c). The oxidation should be induced by the fullerol radical cation (reaction (7)) and the retarded recombination in the presence of Nb dopants should facilitate the oxidative reactions as well (see Scheme 1). Alternatively, the oxidation can be initiated by the hydroxyl radical generated through the reduction of O_2 (reactions (8–10)). Therefore, in the overall photocatalytic process occurring on fullerol/Nb-TiO_2, the anchored fullerol enables the electron transfer from its HOMO to TiO_2 CB via a visible light-induced CT mechanism while the presence of Nb dopants facilitates the electron transport and retards the charge recombination. Both effects cooperate to facilitate the photooxidative as well as the photoreductive conversions under visible light.

The photostability of fullerol/Nb-TiO_2 was evaluated by carrying out the repeated cycles of 4-CP degradation (Fig. 7a) and Cr^{VI} reduction (Fig. 7b). A calculated amount of 4-CP and Cr^{VI} was injected in the same batch of the catalyst reactor every 4 h (for 4-CP) or 1.5 h (for Cr^{VI}). The oxidative degradation of 4-CP and the reductive removal of Cr^{VI} by fullerol/Nb-TiO_2 were stably maintained during the repeated uses of the same batch of the catalyst with exhibiting no significant deactivation. The photochemical stability of fullerol/Nb-TiO_2 is a clear merit in comparison with a typical dye-sensitized TiO_2 that is often unstable in water under irradiation.

The PEC properties were measured using the electrodes coated with catalyst materials and shown in Fig. 8. The photocurrent generation under visible light (Fig. 8a), the normalized time profiles of open-circuit potential (OCP) decay (Fig. 8b), and the electrochemical impedance spectroscopy (EIS) Nyquist plot (Fig. 8c) are compared among bare TiO_2, Nb-TiO_2, fullerol/TiO_2 and fullerol/

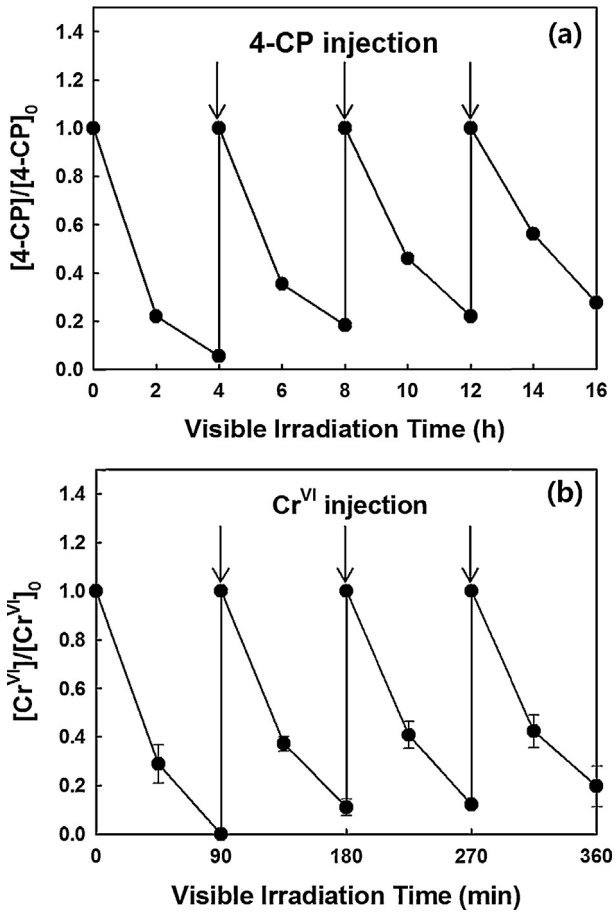

Fig. 7. Repeated cycles of (a) the degradation of 4-CP and (b) the reductive removal of Cr^{VI} under visible light in the same batch of fullerol/Nb-TiO_2 suspension. The experimental conditions were [catalyst] = 0.5 g/L, $[4\text{-CP}]_0$ = 100 μM and pH_0 = 3.0.

Nb-TiO_2. The photocurrent reflects the efficiency of charge pair generation under visible light and the OCP decay after turning off the light represents the charge recombination behavior [42]. The higher the photocurrent, the more charge pairs are generated that survive recombination; besides, the slower the OCP decay, the slower the recombination rate. The photocurrent (or the residual OCP after the light is turned-off) increased in the order of bare TiO_2 < Nb–TiO_2 < fullerol/TiO_2 < fullerol/Nb–TiO_2, which agrees with the photocatalytic activity order (see Fig. 6). The similar correlation between the photocatalytic and PEC activities strongly supports that the origin of the enhanced photocatalytic activity is related with the changes in the electron transfer and recombination properties in the modified TiO_2 systems. First, the fact that both Nb–TiO_2 and fullerol/TiO_2 exhibited higher photocurrent and slower recombination than bare TiO_2 indicates that both Nb doping and fullerol complexation induces the visible light absorption and retards the charge recombination as we discussed previously. The photocurrent obtained with the fullerol/Nb-TiO_2 electrode was the highest, which is consistent with the highest photocatalytic activity. The OCP decay (or recombination rate [43,44]) was also most retarded with fullerol/Nb-TiO_2 (Fig. 8b). The enhanced electron transfer in fullerol/Nb–TiO_2 is also demonstrated by EIS in which the smaller size of the arc in an EIS Nyquist plot indicates the smaller charge–transfer resistance on the electrode surface [45]. As shown in Fig. 8c, the electrode of fullerol/Nb–TiO_2 exhibits the smallest size of arc, which confirms that the charge separation and electron transfer within the fullerol/Nb–TiO_2 electrode is more efficient than those in other electrodes.

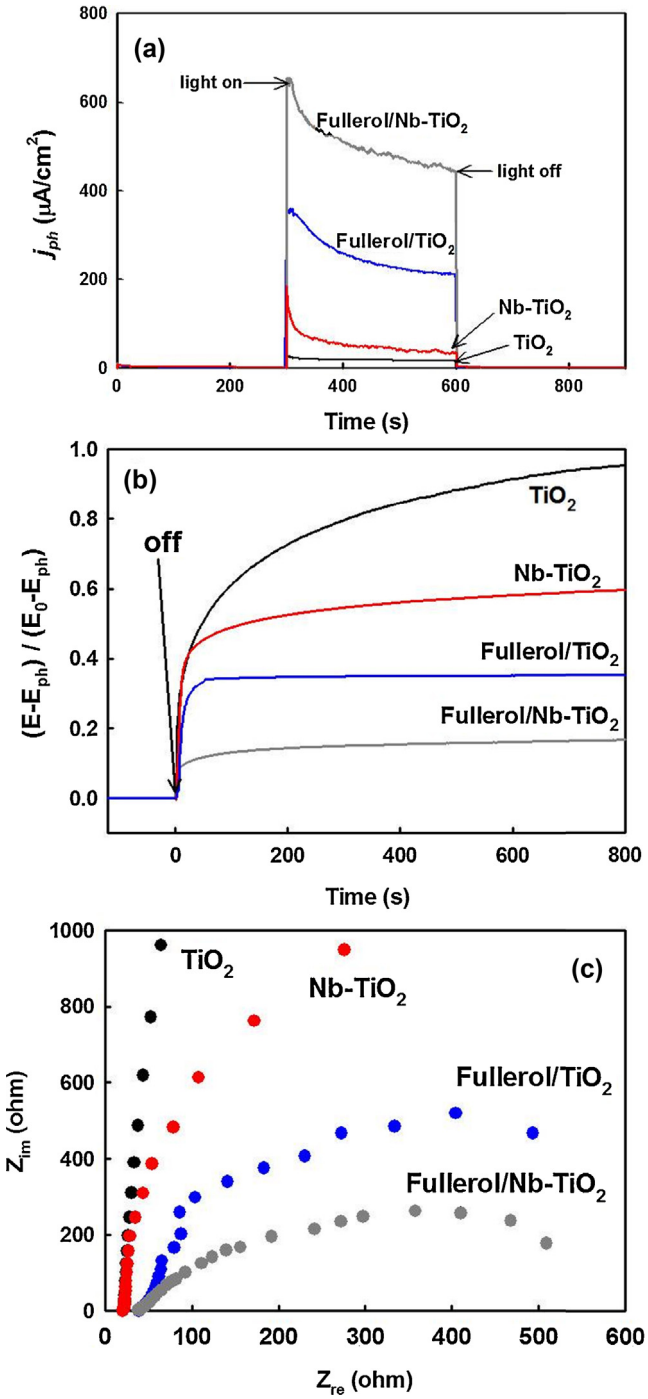

Fig. 8. (a) Photocurrent responses of TiO_2, Nb-TiO_2, fullerol/TiO_2 and fullerol/Nb-TiO_2 electrodes under visible light irradiation, (b) normalized open-circuit potential (OCP) decay curves after turning off the visible light. (E_0: steady-state OCP in the dark, E_{ph}: steady-state OCP under irradiation) and (c) electrochemical impedance spectroscopic Nyquist plots under visible light. The experimental conditions were $[NaClO_4]$ = 0.2 M, pH_i = 3.0, potential bias of +0.6 V (for *a*) and 0 V (for *c*) (*vs.* Ag/AgCl). The electrolyte solution was continuously N_2-purged.

Fullerol sensitizes TiO_2 by CT excitation under visible light while it may serve as an electron trap site (by forming a fullerol anion radical) as well, which not only increases the visible light activity but also retards the charge recombination. On the other hand, Nb-doping enhances the electron transport efficiencies by increasing the conductivity of TiO_2 and retards the charge recombination by trapping electrons at the Ti cation vacancy sites. Therefore, when Nb–TiO_2 was sensitized by fullerol through CT mechanism, the

functions of dual components cowork and enhance the CT-type sensitization efficiency. The Nb-induced defect levels may trap the electron transferred from fullerol to retard the fast charge recombination. All the above photocatalytic and PEC behaviors confirm that the dual modification of TiO_2 by fullerol and Nb dopants markedly enhances the visible light activity.

4. Conclusions

We prepared TiO_2 nanoparticles modified with both fullerol complexes and Nb-dopants to achieve the enhanced CT-type photocatalysis working under visible light. As-prepared fullerol/Nb–TiO_2 was characterized by various analytical methods and tested to evaluate the photocatalytic and PEC activities under visible light. All results revealed that fullerol/Nb–TiO_2 has higher activities as compared to bare TiO_2 and singly modified TiO_2 (*i.e.*, Nb–TiO_2 and fullerol/TiO_2). The visible light photocatalytic activities were well correlated with the PEC behaviors observed under visible light irradiation. Fullerol increases the visible light absorption of bare TiO_2 through the surface-complex CT-mechanism. Nb-doping enhances the photocatalytic efficiency because it not only increased the conductivity of TiO_2 but also retarded the charge recombination by introducing the Ti cation vacancies that act as electron trap sites. By combining the two modifiers of TiO_2, the photocatalytic and PEC activities could be significantly enhanced. Although fullerol/TiO_2 is more stable than dye-sensitized TO_2 in water [15], the visible light absorption by the former is much lower than the latter. By doping TiO_2 with Nb, not only the visible light absorption by fullerol CT-sensitization can be enhanced, but also the interfacial electron transfer can be facilitated with enhancing the overall photocatalytic activity.

Acknowledgments

This work was supported by the Green City Technology Flagship Program funded by KIST (KIST-2012-2E23322), the EPB Center (no. 2008-0061892), the Global Frontier R&D Program on Center for Multiscale Energy System (2011-0031571), and KCAP (Sogang Univ.) (no. 2009-0093880) funded by the Korea government (MSIP) through NRF.

Appendix A. Supplementary data

Supplementary data associated with this article can be found, in the online version, at http://dx.doi.org/10.1016/j.apcatb.2014.01.026.

References

[1] M.A. Henderson, I. Lyubinetsky, Chem. Rev. 113 (2013) 4428.
[2] T. Tachikawa, T. Majima, Chem. Soc. Rev. 39 (2010) 4802.
[3] M.R. Hoffmann, S.T. Martin, W. Choi, D.W. Bahnemann, Chem. Rev. 95 (1995) 69.
[4] H. Park, Y. Park, W. Kim, W. Choi, J. Photochem. Photobiol., C 15 (2013) 1.
[5] Y.N. Huo, Z.F. Bian, X.Y. Zhang, Y. Jin, J. Zhu, H.X. Li, J. Phys. Chem. C 112 (2008) 6546.
[6] G. Wu, T. Nishikawa, B. Ohtani, A. Chen, Chem. Mater. 19 (2007) 4530.
[7] Y. Park, S.H. Lee, S.O. Kang, W. Choi, Chem. Commun. 46 (2010) 2477.
[8] X.H. Zhang, Y. Veikko, J. Mao, P. Cai, T.Y. Peng, Chem. Eur. J. 18 (2012) 12103.
[9] C.W. Cheng, S.K. Karuturi, L.J. Liu, J.P. Liu, H.X. Li, L.T. Su, A.I.Y. Tok, H.J. Fan, Small 8 (2012) 37.
[10] T. Kiyonaga, T. Akita, H. Tada, Chem. Commun. 15 (2009) 2011.
[11] Z.P. Yao, F.Z. Jia, S.J. Tian, C.X. Li, Z.H. Jiang, X.F. Bai, ACS Appl. Mater. Interfaces 2 (2010) 2617.
[12] H.I. Kim, J. Kim, W. Kim, W. Choi, J. Phys. Chem. C 115 (2011) 9797.
[13] H. Park, W. Choi, M.R. Hoffmann, J. Mater. Chem. 18 (2008) 2379.
[14] P. Persson, R. Bergstrom, S. Lunell, J. Phys. Chem. B 104 (2000) 10348.
[15] Y. Park, N.J. Singh, K.S. Kim, T. Tachikawa, T. Majima, W. Choi, Chem.—Eur. J. 15 (2009) 10843.
[16] C. Feng, Z. Weiwei, Q. Wenwu, Z. Jinlong, Catal. Commun. 10 (2009) 1510.
[17] G. Kim, W. Choi, Appl. Catal., B 100 (2010) 77.
[18] J.A. Harris, K. Trotter, B.S. Brunschwig, J. Phys. Chem. B 111 (2007) 6695.
[19] G. Zhang, W. Choi, Chem. Commun. 48 (2012) 10621.
[20] G. Zhang, G. Kim, W. Choi, Energy Environ. Sci. (2014), http://dx.doi.org/10.1039/C3EE43147A.
[21] W. Kim, T. Tachikawa, T. Majima, C. Li, H.-J. Kim, W. Choi, Energy Environ. Sci. 3 (2010) 1789.
[22] W. Kim, T. Tachikawa, T. Majima, W. Choi, J. Phys. Chem. C 113 (2009) 10603.
[23] F.Z. Huang, Q. Li, G.J. Thorogood, Y.B. Cheng, R.A. Caruso, J. Mater. Chem. 22 (2012) 17128.
[24] F.Z. Huang, Y.B. Cheng, R.A. Caruso, Aust. J. Chem. 64 (2011) 820.
[25] T. Nikolay, L. Larina, O. Shevaleevskiy, B.T. Ahn, Energy Environ. Sci. 4 (2011) 1480.
[26] J. Lim, P. Murugan, N. Lakshminarasimhan, J.Y. Kim, J.S. Lee, S.-H. Lee, W. Choi, J. Catal. 310 (2014) 91.
[27] M. Yang, H. Jha, N. Liu, P. Schmuki, J. Mater. Chem. 21 (2011) 15205.
[28] Y. Furubayashi, T. Hitosugi, Y. Yamamoto, K. Inaba, G. Kinoda, Y. Hirose, T. Shimada, T. Hasegawa, Appl. Phys. Lett. 86 (2005) 252101.
[29] X.J. Lu, X.L. Mou, J.J. Wu, D.W. Zhang, L.L. Zhang, F.Q. Huang, F.F. Xu, S.M. Huang, Adv. Funct. Mater. 20 (2010) 509.
[30] A.V. Emeline, Y. Furubayashi, X.T. Zhang, M. Jin, T. Murakami, A. Fujishima, J. Phys. Chem. B 109 (2005) 24441.
[31] A.D. Eaton, L.S. Clesceri, A.E. Greenberg, Standard Methods for the Examination of Water and Wastewater, APAH, Washington, DC, 1995.
[32] Y. Park, W. Kim, H. Park, T. Tachikawa, T. Majima, W. Choi, Appl. Catal., B 91 (2009) 355.
[33] N.J. Bell, H.N. Yun, A.J. Du, H. Coster, S.C. Smith, R. Amal, J. Phys. Chem. C 115 (2011) 6004.
[34] J. Zhong, F. Chen, J.L. Zhang, J. Phys. Chem. C 114 (2010) 933.
[35] D. Morris, Y. Dou, J. Rebane, C.E.J. Mitchell, R.G. Egdell, D.S.L. Law, A. Vittadini, M. Casarin, Phys. Rev. B: Condens. Matter 61 (2000) 13445.
[36] A.M. Ruiz, G. Dezanneau, J. Arbiol, A. Cornet, J.R. Morante, Chem. Mater. 16 (2004) 862.
[37] J. Premkumar, Chem. Mater. 16 (2004) 3980.
[38] G. Zhang, D. Monllor-Satoca, W. Choi, Catal. Sci. Technol. 3 (2013) 1790.
[39] Y.J. Liu, J.M. Szeifert, J.M. Feckl, B. Mandlmeier, J. Rathousky, O. Hayden, D. Fattakhova-Rohlfing, T. Bein, ACS Nano 4 (2010) 5373.
[40] M. Yang, D. Kim, H. Jha, K. Lee, J. Paul, P. Schumuki, Chem. Commun. 47 (2011) 2032.
[41] A. Mattsson, M. Leideborg, K. Larsson, G. Westin, L.J. Österlund, J. Phys. Chem. B 110 (2006) 1210.
[42] T. Berger, D. Monllor-Satoca, M. Jankulovska, T. Lana-Villarreal, R. Gómez, ChemPhysChem 13 (2012) 2824.
[43] D. Monllor-Satoca, R. Gómez, W. Choi, Environ. Sci. Technol. 46 (2012) 5519.
[44] J. Kim, D. Monllor-Satoca, W. Choi, Energy Environ. Sci. 5 (2012) 7647.
[45] Y. Park, S.-H. Kang, W. Choi, Phys. Chem. Chem. Phys. 13 (2011) 9425.